Processing and Filtering of Leaf Area Index Time Series Assessed by In-Situ Wireless Sensor Networks

Jan Bauer[a]*, Thomas Jarmer[b], Siegfried Schittenhelm[c], Bastian Siegmann[d], Nils Aschenbruck[a]

[a] *University of Osnabrück, Institute of Computer Science, Distributed Systems Group*
[b] *University of Osnabrück, Institute of Computer Science, Remote Sensing Group, Wachsbleiche 27, 49090 Osnabrück, Germany*
[c] *Julius Kühn-Institute Braunschweig, Federal Research Centre for Cultivated Plants, Institute for Crop and Soil Science, Bundesallee 58, 38116 Braunschweig, Germany*
[d] *Forschungszentrum Jülich, Institute of Bio- and Geosciences, Plant Sciences (IBG-2), Wilhelm-Johnen-Straße 52428 Jülich, Germany*

Abstract

A precise and up-to-date situational awareness of crop conditions is important for site-specific agricultural management and precision farming, in general. The continuous monitoring of relevant crop parameters has recently been shown to have a great potential and to assist in a large number of applications. In this context, the leaf area index (LAI) is a key parameter that is also used in many other domains beyond precision farming. Its acquisition and assessment are critical for the understanding of many aspects of crop development, the dynamic growth process, and also growth anomalies. However, a continuous monitoring using traditional LAI assessment methods is hardly possible and very expensive. For this reason, low-cost sensors based on Wireless Sensor Network (WSN) technology have been developed and interconnected to agricultural in-situ sensor networks that are promising to estimate LAI with high spatio-temporal resolution.

In this paper, we report on our experience of deploying a long-term crop monitoring sensor network in field plots with different wheat cultivars (*Triticum*

*Corresponding author. Tel.: +49 541 969 7167; fax: +49 541 969 2799.
Email addresses: bauer@uos.de (Jan Bauer[a]), tjarmer@uos.de (Thomas Jarmer[b]), siegfried.schittenhelm@julius-kuehn.de (Siegfried Schittenhelm[c]), b.siegmann@fz-juelich.de (Bastian Siegmann[d]), aschenbruck@uos.de (Nils Aschenbruck[a])

aestivum L.) and water regimes. By a comparative analysis with a commercial LAI instrument, we show that our low-cost radiation-based WSN approach is applicable to wheat and, moreover, is able to differentiate between individual wheat cultivars as well as to detect drought stress. In addition, we present LAI developments over time resulting from continuous estimates for each individual wheat plot, monitored by the sensor network during the relevant time span of the wheat growth period. At the same time, we demonstrate the demand for an adequate filtering and processing of distributed sensor information. Therefore, the non-negligible environmental impact is analyzed and generic filter methods for radiation-based LAI assessment approaches are introduced. Applying these filters, a high correlation with traditional LAI methods is achieved and credible trajectories of LAI development with high temporal resolution are produced. These trajectories appropriately fit the dynamic crop growth process and allow a site- and cultivar-specific differentiation. Thus, the proposed WSN-based LAI monitoring system enables new applications and opportunities. It can greatly support modern crop management and breeding.

Keywords: Wireless Sensor Network, Precision Agriculture, Long-term Deployment, Leaf Area Index, Crop Parameter Monitoring.

1. Introduction

The leaf area index (LAI) is one of the most important bio-physical plant parameters. It is a key enabler for many applications in various disciplines such as ecology, meteorology, climatology and contributes to the understanding of biosphere-atmosphere interactions. For flat-leaved vegetation, LAI is commonly defined as the dimensionless ratio of total on-sided foliage area to ground surface area (Jonckheere et al., 2004). Since LAI is an indicator for physiological and structural functions of canopies and an integrative measure for the photosynthetic performance of plants, it is an appropriate parameter of crop growth during the complete phenological cycle. In the context of precision agriculture, LAI assessment can be useful for the early detection of growth

tendencies and anomalies. Hence, LAI provides essential information for yield models and, therefore, also serves as an indicator for yield-reducing processes caused by diseases or mismanagement (Carter, 1994).

An earlier and more precise site-specific knowledge of individual dynamic growth processes in agricultural fields will produce valuable insights for farmers. As a result, this knowledge will positively influence modern agricultural practices and also improve the prediction of yield rates. Thus, it is crucial to increase farm output and at the same time to reduce waste and to ensure sustainability, in particular in the domain of irrigated agriculture which will become more and more important due to the emerging effects of the climate change. For the realization of such a timely situational awareness with a high spatio-temporal resolution, there is a steadily increasing demand for in-situ environmental monitoring by advanced Wireless Sensor Network (WSN) and Internet of Things (IoT) technology. Aside from soil and moisture properties, the exploration of bio-physical and bio-chemical crop parameters like fractional cover, biomass, fraction of absorbed photosynthetically active radiation (fPAR), and first and foremost LAI with high-quality, long-term consistent LAI products are of special interest in the context of precision agriculture.

WSNs are composed of a large number of small, cheap, resource- and power-constraint devices that are, depending on their sensing task, equipped with one or multiple sensors (Akyildiz et al., 2002). These devices are wirelessly interconnected, typically in a self-organizing manner, within a local network and responsible for data transmission and often data forwarding to a central IoT base station, possibly connected to the Internet. The main purpose of each individual device in such a network is the environmental sensing of physically measurable phenomenas, e.g., temperature, relative humidity, or soil moisture. Precisely because of the low-cost and low-power characteristics of individual devices, they are suitable for large-scale and long-term deployments. The downside of this resource-constraint is that these typically battery-driven devices have limited sensing accuracy only. However, this limitation is compensated by the large number of collaborating devices, which are able to continuously provide sensor

information at high temporal as well as spatial resolution. Hence, WSNs are particularly tailored for ground-based monitoring of crop parameters as has been realized by research since more than one decade now. A promising progress has already been made for WSN-based LAI assessment and the potential to reduce time and labor costs of conventional in-situ acquisition has been shown (e.g., Yuan et al., 2009; Shimojo et al., 2013; Qu et al., 2014a; Bauer et al., 2016). Moreover, WSNs beneficially assist the validation and improvement of phenological models and parameter maps or other products derived by remote sensing. Using satellite or aerial imagery collected by drones, LAI information gathered by in-situ WSNs can be extrapolated and scaled-up to large areas (e.g., Qu et al., 2014b). However, particularly regarding the crop LAI, current accuracy, consistency, and temporal resolution may not meet the requirements from the application viewpoint of agricultural end-users.

In this paper, we continue our previous work (Bauer et al., 2016) that proposes a low-cost LAI sensor prototype and realize a long-term LAI monitoring system. The core contributions are:

- A method for processing and filtering WSN data is introduced that is necessary to obtain feasible high-resolution LAI time series. We present this along with experimental results achieved by our system and a comparative analysis with a commercial LAI device.

- The following research question is answered: Can yield-limiting tendencies as well as cultivar-specific differences of crop growth processes reliably be described by WSN-based LAI monitoring systems?

2. Background

2.1. A Brief Review on Conventional LAI Assessment

Direct methods to assess LAI provide the most reliable and precise results. A common approach is to destructively assess this index by manually collecting all leaves in a reference plot and measuring their individual areas directly

using planimeters. But also allometric approaches exist, avoiding the harvesting of plants. Nevertheless, direct methods are extensively time- and labor-consuming, and, thus, costly and limited to small areas (Bréda, 2003; Jonckheere et al., 2004). Therefore, various indirect and non-destructive methods have been developed that derive LAI indirectly by measuring a certain related quantity, usually the transmittance of solar radiation through the canopy. Existing indirect methods differ in many aspects and can be grouped into in-situ and remote sensing approaches. Traditional in-situ methods use specific instruments with passive optical sensors that are commercially available, most notably AccuPAR (Decagon Devices), LAI-2200 (LI-COR Bioscience), and SunScan (Delta-T Devices). These instruments allow a manual estimation of LAI in the area of interest (Jonckheere et al., 2004; Weiss et al., 2004; Bréda, 2003), but corresponding measurements are conducted in a point-by-point manner bearing the risk of being influenced by changing weather conditions. In the recent years, the traditional ground-based assessment is complemented by digital hemispherical photography (DHP) approaches that use upward-pointing digital cameras (e.g., Ryu et al., 2012) to derive LAI from digital imagery.

Complementary to in-situ methods, LAI derived from remote sensing multi- and hyperspectral imagery enabled by satellites or recently by drones, represents an established indirect alternative. However, for model calibration, validation, and training of remote sensing products, in-situ measurements are still necessary and conducted in practice (cf. e.g., Boegh et al., 2002; Qu et al., 2014b). Overall, common shortcomings of all conventional methods, in-situ and remote, are high costs, either in terms of labor costs of manual measurements or monetary costs for high-resolution satellite imagery. Moreover, manual measurements or drone campaigns are usually conducted sparsely. On the other hand, satellite imagery is prone to adverse weather conditions. Hence, conventional LAI assessment has a relatively low temporal and/or spatial resolution that might not meet the requirements of possible applications in field-phenotyping and precision agriculture.

2.2. WSN-based LAI Monitoring

Technological advancements highly reduced the physical size and costs of sensors enabling them to be used in large-scale wireless networks for many applications in a variety of domains. Using environmental sensors, WSNs gradually complement existing monitoring systems in the context of precision agriculture with ground-based information to increase productivity and sustainability. Possible applications range from site-specific irrigation, fertilization, and crop treatment, to horticulture and animal monitoring (Rehman et al., 2014). Nowadays, they are often integrated into farm management information system (FMIS) and IoT platforms, such as FarmBeats (Vasisht et al., 2017), for instance.

Pioneer research of non-destructive WSN-based LAI assessment is shared by Yuan et al. (2009), proposing an iterative scheme to deploy sensors into farmland and a processing of sensory data taking vary light reflections and refractions into account. Shimojo et al. (2013) introduce a continuous LAI monitoring system and demonstrate the feasibility of commercial off-the-shelf (COTS) sensors for LAI estimation in a tomato greenhouse. Another progressive system, LAINet, based on a specific multi-point optical sensor system is presented by Qu et al. (2014a) who also show preliminary research on the validation of remote sensing products using WSNs (Qu et al., 2014b). As recent work (Qu et al., 2014a) and also the absence of mentioning in current reviews (Rehman et al., 2014) reveal, WSN-based LAI assessment is still in an emerging stage. However, its potential and opportunity to enable multi-point monitoring systems and at the same time to overcome the shortcomings of traditional point-by-point measurements have been repeatedly shown.

2.3. LAI Estimation

In our previous work (Bauer et al., 2016), we presented a novel low-cost sensor for a radiation-based LAI assessment and show the feasibility of the sensing system and promising results in maize (*Zea mays* L.) cultivars. The developed prototype enhances a COTS photosynthetically active radiation (PAR)

sensor platform with a diffuser and special optical filter. Following a simplistic approach, the sensor is not assumed to deliver more accurate results than commercial instruments. However, due to the potentially large number of replicated measurements and distributed sensors, a continuous monitoring with fine-grained temporal resolution during the entire crop growing cycle is enabled.

Similar to the approach of Shimojo et al. (2013), we use the Monsi-Seaki model (Monsi and Saeki, 1953). This simplified model is based on the inversion of the Beer-Lambert law and, under certain assumptions (cf. Weiss et al., 2004)), derives LAI estimates from the transmittance T of solar radiation through the canopy. The relation can be formulated as:

$$LAI = -\omega \; ln(T) = -\omega \; ln\left(\frac{B}{A}\right), \tag{1}$$

where T is obtained be the ratio of perceived radiation below (B) and above (A) the canopy. Thus, basically two measurements and sensors, respectively, are necessary to estimate LAI. However, the indirect assessment is very complex in practice and there are many other parameters that influences this estimation such as the solar zenith angle (SZA) and weather factors, for instance. Accordingly, a correction factor ω is used to rectify the reverse exponential relation between LAI and transmittance. This factor is cultivar- and site-specific and, among others, mainly affected by the SZA and the canopy structure, particularly leaf distribution, mean leaf angle (MLA), and clumping. In general, ω is unknown but can be determined empirically, as already done for maize and our prototype (Bauer et al., 2016). However, for winter wheat, ω is not yet identified. Thus, it is initial assigned with $\omega_{initial} = 1.24$ here, which is inspired by a parameter set of the LAI-2200 (cf. Bauer et al., 2016) and later adjusted using a comparative analysis with the SunScan instrument introduced in the following section.

Another noteworthy aspect is that neither the developed sensor prototype nor the SunScan instrument is able to measure the actual true LAI due to the presence of non-photosynthetic canopy elements such as branches and stems that cannot be distinguished adequately. Thus, several alternative terms have been

proposed to describe the estimates obtained by those and similar approaches, most notably the terms plant area index (PAI) and effective LAI (cf. Jonckheere et al., 2004). However, in this paper, we still use the term LAI for consistency, but distinguish between the so-called green LAI (GLAI). It refers to the sampling strategy in which yellow leaves in progressing phenological stages are intentionally excluded from PAR measurements in order to focus on the photosynthetically active leaf area.

2.4. Reference Instrument and Ground Truth Data

Ground truth LAI estimates are assessed by regularly measurements using the SS1 SunScan, a widely-used canopy analyzer that is optimized for agricultural crops with low regular canopies. The instrument is also radiation-based and has a 1 m probe with an array of 64 PAR sensors to measure the transmittance. The additional radio-linked BF3 Sunshine Sensor is used for simultaneous reference sampling. LAI measurements were conducted on nine selected days during the wheat growth period, each around noon under stable weather conditions (sunny and unclouded) according to the GLAI sampling strategy, i.e. by holding the probe just below the green leaf layer.

3. WSN Architecture & Deployment

3.1. Deployment Site

The deployment site is located at Braunschweig, Germany, on experimental fields of the Julius Kühn-Institute (JKI) (52.296° N, 10.436° E; 75 m elevation). During the 2016 growing season, the maximum impact of water shortage and drouth stress on wheat phenology, physiology, and yield was investigated. Therefore, different wheat cultivars were grown: (1) in a mobile rain-out shelter (dry environment; referred to as ROS) and (2) in a nearby irrigated control (wet environment; referred to as CON). The ROS is a foil covered shelter (cf. Fig. 1(a)) that automatically moves over the experimental plots during rainfall periods via a rail system. For further details of the ROS site refer to Schittenhelm et al. (2014). The main WSN deployment was operating

(a) ROS with Hystar and Gordian plots at DOY 178 (sensors 0x1, 0x2, 0x5, 0x6).

(b) CON with Hystar and Gordian plots at DOY 105 (sensors 0x3, 0x4, 0x7, 0x8).

(c) Above reference sensors (0xA, 0xB)

Figure 1: Sensing regions at different locations.

for 74 days in 2016 (day of year (DOY) 105 – 178). Two particular high yielding wheat cultivars were observed, each in the ROS (Fig. 1(a)) and the CON field (Fig. 1(b)). The first one is Hystar (referred to as cultivar 1), an early maturing hybrid wheat, and the second one is Gordian (referred to as cultivar 2), a cultivar with medium maturity.

3.2. Real-World Challenges

The main reasons of challenges for outdoor deployments in the agricultural domain can be grouped into two categories: (1) environmental and (2) wildlife induced challenges. Our key approach in order to cope with both types of challenges is remote monitoring of all components and redundancy (cf. Bauer and Aschenbruck, 2018). For the radiation-based LAI assessment, two essential measurement positions are required: a ground sensor below the canopy and a corresponding above reference sensor (Fig.1(c)). For redundancy, three above references are used and, in each cultivar, two ground sensors are deployed. Moreover, wireless (IEEE 802.15.4) and wired (USB) connections are used in order to increase redundancy of data delivery. While there is a power source available at the ROS, solar power solutions had to be used for the CON area and the above reference sensor stand. Unfortunately, the installed solar panel and

(a) Condensation water under the diffuser cap of sensor 0x7 (DOY 178).

(b) Condensation water under the diffuser cap of reference sensor 0xB and traces of bird droppings (DOY 125).

Figure 2: Impressions of a certain impact of harsh outdoor environments on WSN equipment.

batteries were not fully reliable and led to temporary disruptions of the deployment. Furthermore, it turns out, that sensor cases were not completely sealed and water-resistant. As a consequence, condensation water occurs under the diffuser cap of some sensors, cf. Fig. 2. Suchlike challenges could easily be mitigated by industrial outdoor cases, enhanced solar power equipment, and professional uninterruptible power supply systems. However, it is hardly possible to tackle all challenges which potentially could arise in real-world deployments. In practice, a non-disruptive WSN operation could not be guaranteed and erroneous sensors could never be totally prevented. Thus, we believe that sensor redundancy is the most reasonable approach to cope with adverse and unpredictable situations. Hence, it is crucial to realize a low-cost sensing platform as proposed with our COTS prototype.

3.3. Architecture

According to the concept described by Bauer and Aschenbruck (2018), clusters of four sensor devices that are attached to a Raspberry Pi via USB are used for individual wheat plots. These clusters are connected to a central base station using IEEE 802.15.4 and for redundancy purposes also interconnected in a WLAN. The concrete setup is sketched in Figure 3 and a key data overview of

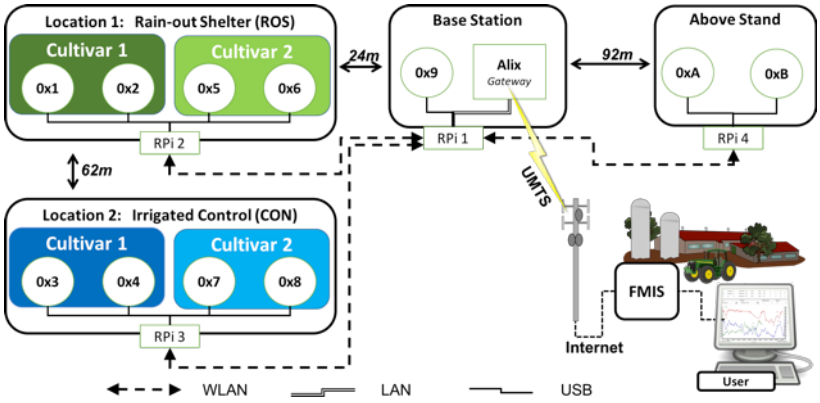

Figure 3: Communication architecture of the deployment. Three self-sufficient sensing clusters are connected via WLAN links with a central gateway node providing UMTS-based Internet connectivity and FMIS integration.

the deployment is given in Table 1. Using public land mobile networks (PLMN) connectivity (i.e. UMTS cellular network), the base station acts as Internet gateway. It is responsible for sensor data upload and also for remote access to the WSN. The overall architectural concept consists not only of the WSN itself, but also of a server that offers web-based monitoring, a database system, and allows remote reconfiguration and reprogramming. It is noteworthy, that the goal of our deployment is neither to realize a complete and mature productive system, nor a sophisticated and efficient WSN. Instead, a functional sensing system that demonstrates the feasibility of providing a continuous LAI monitoring is developed. Furthermore, by intentionally oversampling PAR, our aim is to gather an extensive data set in order to analyze factors influencing LAI estimation.

3.4. Hard- and Software

The low-cost IEEE 802.15.4/ZigBee compliant sensor prototype introduced in our preliminary work (Bauer et al., 2016), i.e. a TelosB-based platform (8 MHz TI MSP430 MCU, 10 kB RAM) is used as basic sensor. Amongst other onboard-sensors, the COTS platform features an appropriate PAR sensor, S1087-1, man-

Table 1: Deployment overview.

Date	2016/04/14 – 2016/06/26 (DOY 105 – 178)
Duration	74 days
# locations	2 (ROS and CON)
# cultivars	2 (Hystar and Gordian)
# sensors	11 (8 ground + 3 reference sensors, 2 sensors/plot)
Sampling rate	30 samples/hour
Sampling phase	21 hours/day (03:00 – 00:00)
Night phase	3 hours/day (00:00 – 03:00)
Max. # samples/sensor	Per day: 630 (68 kB), overall: 46 620 (≈5 MB)
Overall data volume	77.3 MB (incl. additional error logs)

ufactured by Hamamatsu. For a proper LAI assessment, the sensor was enhanced by two essential components: (1) a diffuser cap improving the stability of PAR readings and (2) a blue band-pass filter to select the blue spectrum of visible light and, thus, increase the contrast between green vegetation and sky. Details concerning this setup can be found in (Bauer et al., 2016). The raw sensor readings can be converted into the unit lux according to a formula provided by the manufacturer. However, due to the sensor modification, a recalibration would be necessary. Because such a conversion is not required for the measurement of the transmittance, it is left out here. For convenience, we still use the term PAR readings for unconverted and also filtered digital raw readings obtained by the sensor.

Similar to Mo et al. (2009) and Qu et al. (2014a) and prior to the deployment, a relative calibration was conducted in a controlled laboratory environment by mutual determination of correlation coefficients assuming a linear relation of the solar radiation response between all sensors. Therefore, sensor 0x1 was arbitrarily selected as reference sensor. This calibration is particularly important because of the possible production deviations of sensor cases and modifications.

The basic acquisition software is also adapted from the sensing application introduced in Bauer et al. (2016). In the modified version, the sensor node uses a constant sampling rate of 30 samples/h. Amongst others, each sample consists of multiple PAR sensor readings that are taken in a short burst of 25 readings

with a spacing of 50 ms. This is done in order to get more reliable averages and also to observe small-scale fluctuations. To differentiate between a single PAR samples in such a PAR bundle, the former is hereinafter referred to as PAR reading. The term PAR sample is used for the arithmetic mean of a bundle. As a reliable operation of various components during the entire deployment is explicitly not expected, certain safety mechanism have been implemented. Details can be found in Bauer and Aschenbruck (2018).

3.5. Sensor Data Set

A holistic overview of the entire PAR data collected in the WSN deployment is shown in Figure 4, visualizing data streams of all sensors involved. Each stream has a daily pattern that follows the daily course of the sun, i.e. the increasing solar irradiation in the first half of the day and decreasing irradiation in the second half, both naturally weakened by atmosphere and sky conditions. Due to the unforeseen power supply challenges, the WSN part in the CON plots (cf. Fig. 3), started its operation with a certain delay, at DOY 125 (upper x-axis), still timely to monitor relevant vegetative changes. The overview in Figure 4 provides a first impression of the quantity of data, but also of the data gaps due to the harsh environment and technical problems. It turns out, that the redundancy in our design was actually necessary in many situations. Moreover, it can be seen by the irregular and fragmentary data streams of ROS sensors (green shaded) that there were software issues in the beginning phase of the deployment (DOY 105 – 119) that could be successfully fixed. However, irregularities of CON sensors (blue shaded) are often caused by the under-dimensioned solar power equipment. In fact, the prototypical deployment clearly leaves room for improvement, but still approx. 40 to 80 % of theoretically possible samples were successfully delivered to our database, as noted in Figure 4. Thus, an extensive data set is available.

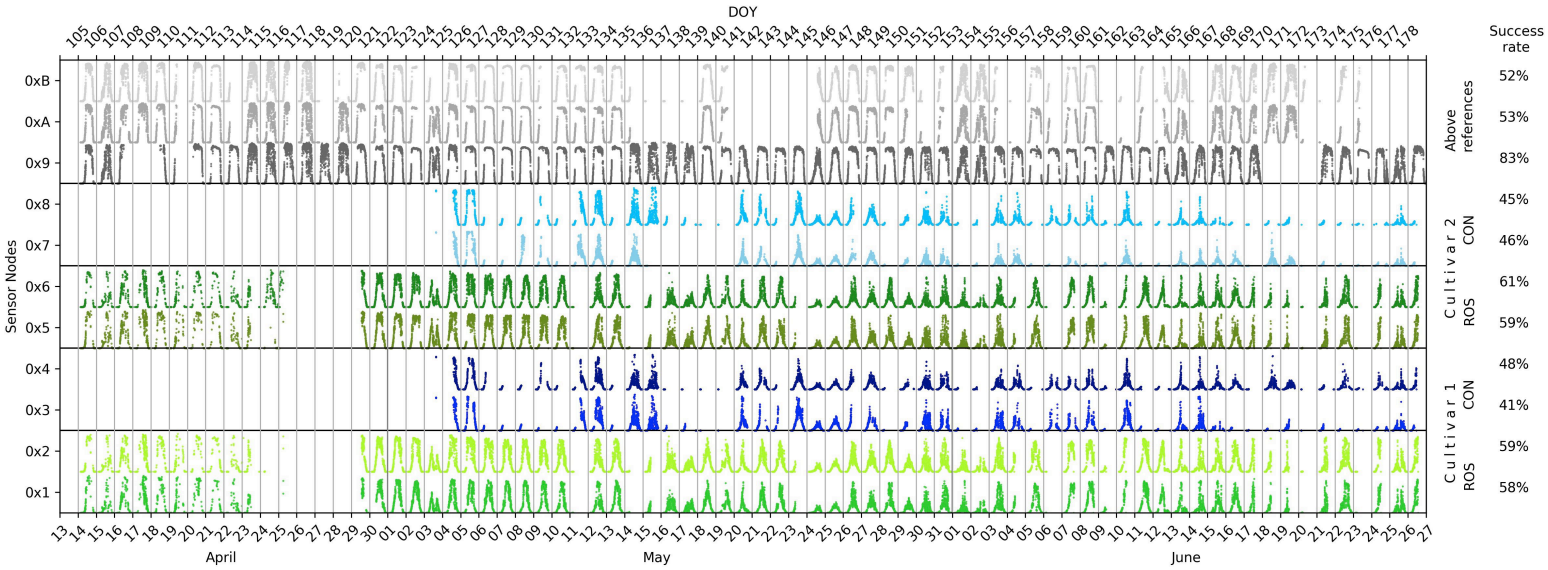

Figure 4: Data overview. Overall visualization of all PAR time series gathered by individual sensors within the relevant part of the wheat growth period grouped in sensor locations.

4. Methodology

For the evaluation of the experimental WSN-derived LAI estimates, a comparative analysis to estimates manually measured with the SunScan instrument briefly introduced in Section 2.4 is conducted. These measurements are seen as (substituted) ground truth for the validation, cf. Sec. 2. Assuming a linear correlation between both set of estimates, we use the Pearson product-moment correlation and a linear regression to compute the correlation coefficients. Hence, the key metric to evaluate the quality of our results is the coefficient of determination r^2 representing the level of agreement with the SunScan values. But also other numerical parameters are considered as the slope α and the interception β of the regression line, as well as the normalized RMSE (nRMSE) defined as $nRMSE = RMSE/(max(LAI_{WSN}) - min(LAI_{WSN}))$.

The WSN deployment produced a large amount of data during the relevant part of the growing season of wheat cultivars observed in this paper. Each individual sensor provides data streams containing various information. For LAI assessment, the only relevant information is the PAR bundle of each sample. Hence, the data processing is limited to these bundles and the data analysis to LAI information, respectively. The entire data processing and analysis can be clustered into six major phases as illustrated in Figure 5. The most challenging part is an appropriate processing chain from raw sensor samples to usable LAI estimates. First, raw samples need to be adequately preprocessed and filtered. Then, preliminary LAI values can be estimated that subsequently need to be post-processed before they can be reasonably compared to ground truth data in the closing comparative analysis. LAI estimates are derived according to the simplified method in Equation 1 (Sec. 2.3) using a multi-angle approach. That means, PAR measurements are conducted over the entire day with different solar incident angles and daily averages involving the entire SZA range are computed. Apart from evaluating the quality of WSN-based LAI estimates by the comparative analysis and the impact of data processing and filtering, a secondary goal is to specify a proper correction factor. Based on the α param-

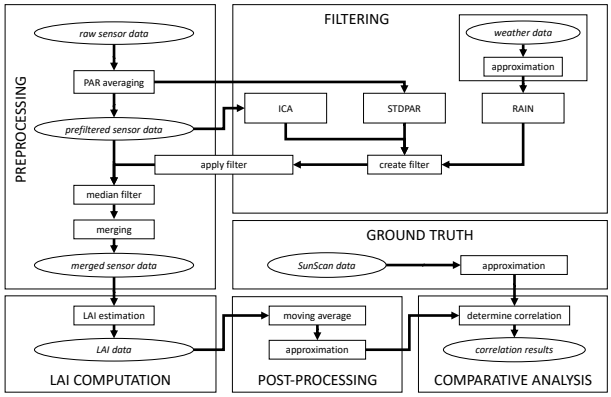

Figure 5: Processing flow diagram: The processing and filtering chain from raw sensor data to reasonable LAI estimates and their comparative analysis with SunScan data.

eter achieved by the sufficient correlation, the initial assignment of ω could be calibrated, provided that the WSN data is processed adequately.

In order to link LAI data with weather information, we benefit from the close proximity (approx. 1 km) of the JKI site to the Agrometeorological Research Centre of the Deutscher Wetterdienst (DWD). We use the weather observation data of this official weather station (ID 662)[1] which is freely available in hourly resolution. The SZA is calculated based on the longitude, latitude, and local sampling time.

5. Data Processing

5.1. Preprocessing of WSN raw data

The first step of the preprocessing phase is the calibration of individual sensor data using the calibration factors, determined a priori as mentioned in Section 3.4. Nevertheless, due to the real-world nature of gathered sensor readings, (calibrated) raw data could be very noisy. On the one hand, reasons could be small-scale environmental noise (in $<$ seconds range) as induced by measurement inaccuracies of individual sensors or by fluctuations below the canopy caused by wind. This challenge is mitigated by averaging multiple consecutive

[1] ftp://ftp-cdc.dwd.de/pub/CDC/observations_germany/climate/hourly

PAR readings of each bundle in each measurement sample (cf. Sec. 3.4). Using this average, a simple minimum threshold (*PARTHRESH*) is applied that eliminates readings in the very low illuminance intensity range. This is because these readings are likely to not provide reliable information because intensity is too low for the ADC resolution as already noticed by Shimojo et al. (2013). We use a minimum of 35 (raw unit) here. On the other hand, there is large-scale noise (in minutes to days range) unavoidably induced by unstable weather conditions as also indicated by existing research (Qu et al., 2014a) or even by single leaves adversely covering sensor caps for a certain period of time, for instance. This kind of noise requires a processing of adjacent samples. For that purpose, we decided to apply a median filter for data smoothing and determined a window size of 11 (i.e. five adjacent samples and in an overall period of ±10 min) to be reasonable to smooth consecutive (averaged) PAR samples.

The reason of deploying sensor pairs in every wheat plot and using three above reference sensors, respectively, is basically redundancy for failure safety. However, if readings from different sensors are appropriately merged, pairwise sensor readings can also enable noise mitigation and, thus, improve data quality. To merge sensor pairs, we use the smoothed data and differentiate between below and above sensors. For the above sensor triple, we use the *maximum* function for merging because these sensors are intended to measure the maximum illuminance intensity of the unobscured sky. Hence, if a single reference sensor is affected for any reason, it has no negative impact on the merged data. Thus, the maximum function ensures that the merged data is not impaired as long as at least one of the above sensors provides reasonable readings. This feature is very crucial since unstable cloudiness or obstacles in the surrounding area can result in situations where some sensors were more shaded than others. Moreover, in our scenario, we occasionally observed birds of prey sitting on the sensor stand (cf. Fig. 2(b)) and heavily obscuring above sensors.

Figure 6 visualizes the very strong linear correlation of individual sensor readings of above reference sensors that are calibrated but not yet smoothed as a scatter plot. Only a slight deviation between readings from sensor 0xA

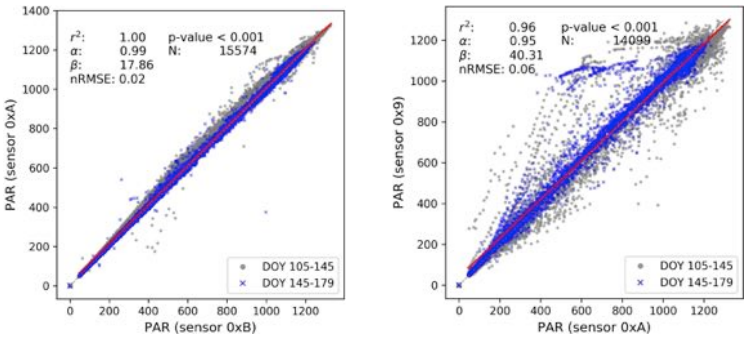

(a) Above sensors (0xA, 0xB), located next to each other.

(b) Above sensors (0x9, 0xA), spatially distributed (92 m).

Figure 6: Pairwise correlations of calibrated PAR samples from above reference sensors.

and 0xB, that both are located on the stand very close to each other, can be observed (Fig. 6(a)) and only a very few outliers exist, probably induced by birds sitting on the stand. This additionally confirms that the sensor a priori relative calibration is effective. Moreover, the PAR data set is divided into data from the first half (gray) and from the second half of the deployment (blue). Regarding the condensation water under the diffuser cap of sensor 0xB (cf. Fig. 2(b)) that arose during the first half, it turns out that the adverse impact of condensation water is very limited. Indeed, the corresponding readings of the affected sensor turned out to be only a little attenuated as the data of the first half (blue) reside mainly slightly above the regression line (red). After detecting the condensation water problem at DOY 125, we re-sealed the sensor leading to the very high correlation in the second half of the deployment.

In contrast to the strong similarity of sensor 0xA and 0xB, the correlation of sensor 0x9 and 0xA (Fig. 6(b)), and 0x9 and 0xB vise versa, shows more anomalies. Here, the impact of sensor 0x9's proximity to the ROS with its shading or reflections can be observed by the distributed outliers below the regression line. Additionally, the impact of trees in the vicinity of the 0xA-0xB sensor stand that result in occasional shading of both sensors, most notably at higher SZAs, can be seen by the structured outliers above the regression line,

and, hence, leading to an overall asymmetrical outlier pattern in this figure. In general, there is a high consistency across all above sensors and the *maximum* function for merging appears to be an appropriate choice.

With regard to the merging of below sensor pairs, the maximum function is not reasonable since it would intensify the impact of outliers. The same would apply in case of the minimum function. We found the *arithmetic mean* of (roughly) simultaneously measured readings to be an appropriate function for merging that kind of sensor information. Although a strong linear correlation can be observed again, there is an apparent difference between below readings of individual sensors at the same location and in the same cultivar induced by small- and large-scale noise and crop heterogeneity. This difference is exemplarily shown for both sensors deployed in cultivar 1 in the ROS by a scatter plot in Figure 7(a). Even though there are extreme outliers in sensor readings, these outliers are pretty symmetric since the regression line lies relatively close to the 1:1 line which further justifies the *arithmetic mean* function for merging. As the subsequent analysis and plausibility checks of all sensor readings revealed, there is one exception in our deployment where an imbalance within a sensor pair exists. In the irrigated control (CON) cultivar 2 plot, there is a significant deviation of sensor 0x8, as demonstrated in Figure 7(b). The reason of the deviation is unclear and might be the result from an incorrect calibration or an adverse positioning of the sensor. However, we believe that this kind of inaccuracy will be likely in large-scale productive WSN systems. Thus, we decided to not exclude the impaired sensor from our comparative analysis, but occasionally refer to results that do not include the possible errors from sensor 0x8 in order to highlight the achievable potential of WSN-based LAI monitoring.

Excluding the exception mentioned above, the pairwise scatter plots of calibrated PAR samples from below sensors in Figure 7 allow additional insights into the great potential of our approach: The choice of particular sensors for the pairwise comparison does characteristically influence the correlation coefficients, most notably r^2 as demonstrated in Figure 8. That means, there is a cultivar-specific difference between the correlation of sensors in different cultivars at the

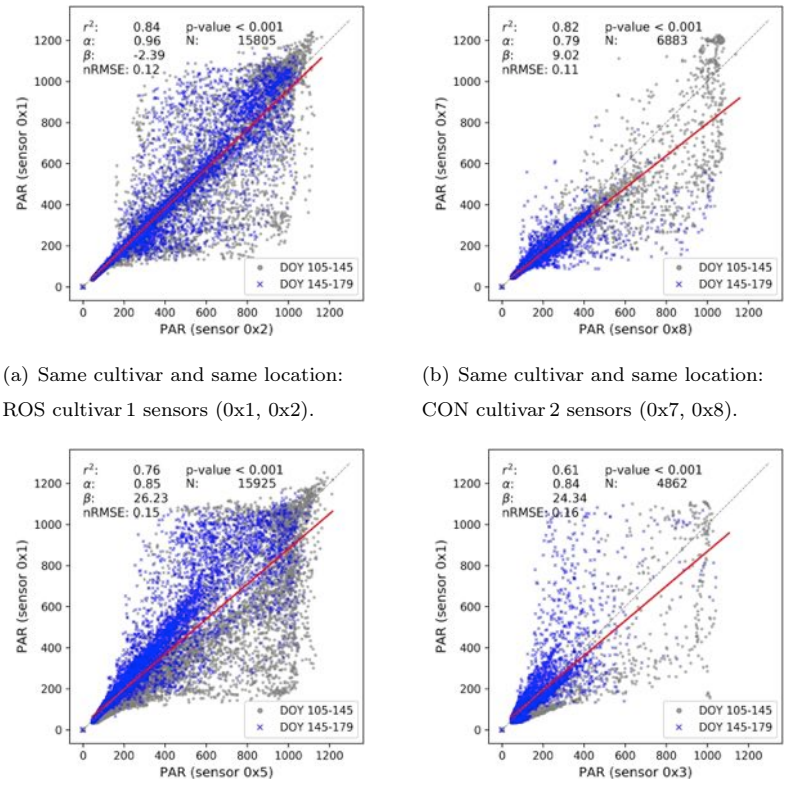

(a) Same cultivar and same location: ROS cultivar 1 sensors (0x1, 0x2).

(b) Same cultivar and same location: CON cultivar 2 sensors (0x7, 0x8).

(c) Different cultivars and same location: ROS cultivar 1 vs. 2 (0x1, 0x5).

(d) Same cultivar and different locations: ROS vs. CON cultivar 1 (0x1, 0x3).

Figure 7: Pairwise Correlations of calibrated PAR samples from below sensors.

same location compared to sensors in the identical plot (same cultivar, same location), cf. Fig. 7(a) vs. (c) and Fig. 8. Moreover, this difference is more significant if sensors within the same cultivar but in different sensing locations are considered (same cultivar, different locations), cf. Fig. 7(d) and Fig. 8. Thus, it already appears that our approach is able to distinguish between the cultivar-specific crop growth characteristics (cultivar 1 vs. 2) and the location-specific difference in growth trajectories induced by drought stress within the ROS. In both cases, there is a noteworthy difference with regard to the DOY when readings are gathered. Whereas readings from the first half (gray) in Figure 7 do not

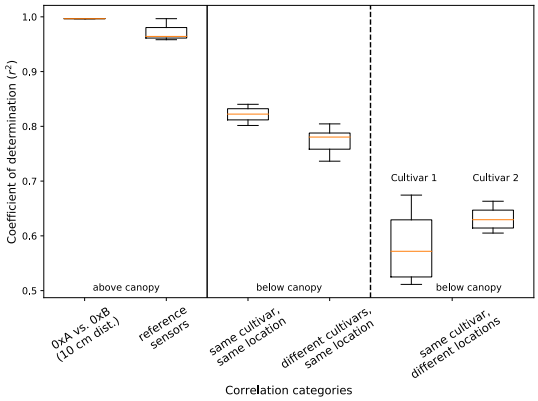

Figure 8: Pairwise correlations of calibrated PAR samples from sensors in different correlation categories and the potential to differentiate between wheat cultivars (same vs. different cultivars) and sensing location (same vs. different locations).

essentially differ from readings of the second half (blue) concerning their symmetry, there is a clear mismatch in symmetry of both classes if both sensors are positioned in different cultivars and/or locations. This observation additionally confirms that cultivar- and location-specific differences are provoked by drought stress. Finally, the differentiation between both cultivars in Figure 8 (same cultivar, different locations) reveals different characteristics of both cultivars. A lower variance and a higher median of the determination coefficient is achieved by cultivar 2 if samples from ROS and CON are compared. Hence, in this experiment, cultivar 2 (Gordian) performs better in the harsh ROS environment regarding the LAI.

5.2. LAI-Estimation

Given the preprocessed PAR samples that have been calibrated, smoothed, and merged, LAI estimation for each wheat plot is straight-forward. LAI estimates can be easily derived by the generic formula in Equation 1 (Sec. 2.3) using samples of the same interval of merged below sensor readings and the corresponding above reference readings along with the preliminary correction parameter $\omega = 1.24$. However, this results in preliminary LAI estimates only, that possibly highly vary over the time of day, as exemplarily demonstrated by different daily snapshots visualized in Figure 9. In the upper part of each subfigure, merged PAR samples of each position are plotted over the time of

the day, i.e. all wheat plots and the corresponding above reference (black). The resulting LAI estimates are included in the lower part (second y-axis). The snapshots already provide a first impression for the daily LAI variance and also indicate that this variance is very weather-depending. On sunny and unclouded days (cf. Fig. 9(a)) there is a very pronounced daily pattern, namely the daily low of decreased LAI estimates from roughly 09:00 to 18:00. If the weather is cloudy or rainy, the daily LAI time series are apparently much more stable (cf. Fig. 9(b) and (c)). Consequently, LAI variance changes accordingly, if weather conditions are changing on days with variable weather (cf. Fig. 9(d)). Another aspect that can be observed in Figure 9(b) is the effect of the ROS that covers the corresponding wheat plots during periods with rainfall, resulting in an invalid LAI increase on the ROS site.

In conclusion, the daily LAI variance shows that it is very reasonable to link sensor data with weather information and to investigate the environmental factors that dominate the weather-dependency. Moreover, it is important to note that a suitable post-processing of daily LAI estimates is necessary to reduce potential noise and smooth LAI time series in order to obtain meaningful growth trajectories.

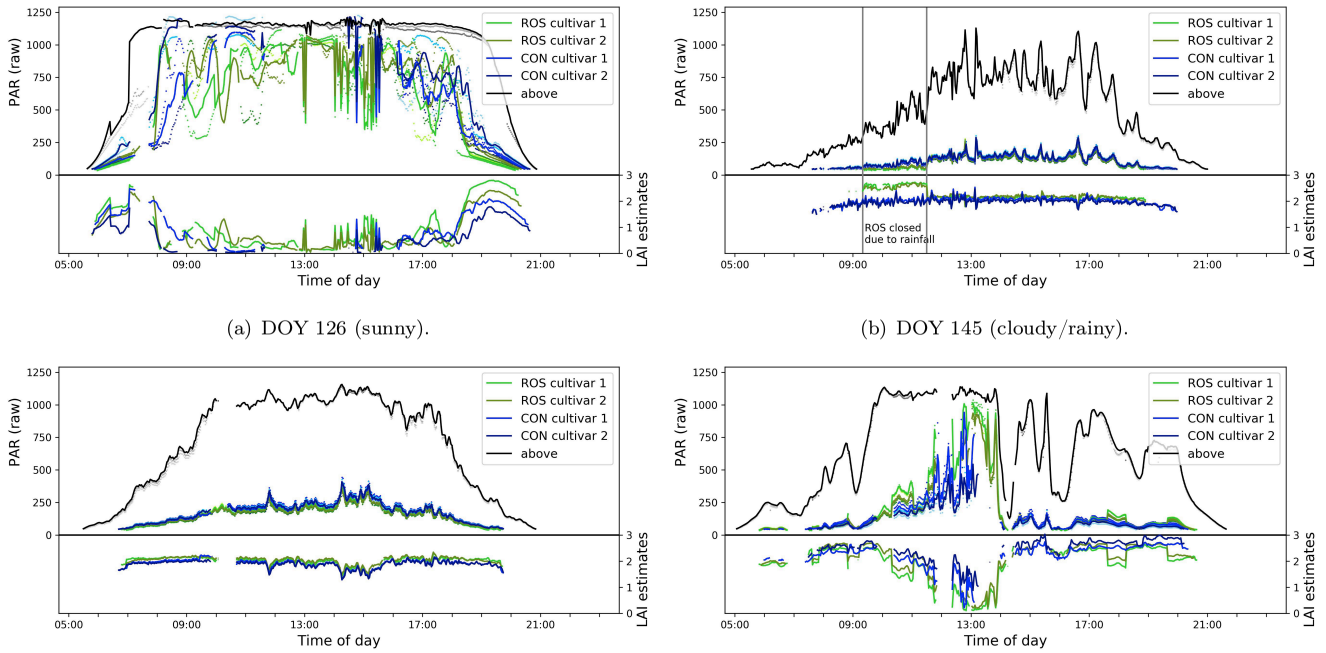

(a) DOY 126 (sunny).

(b) DOY 145 (cloudy/rainy).

(c) DOY 146 (cloudy).

(d) DOY 165 (variable).

Figure 9: Exemplary daily LAI time series on days with different weather conditions.

5.3. Post-Processing and Ground Truth Preparation

The SunScan estimates, serving as ground truth reference, are available for certain days in the wheat growth period only, as described in Section 2.4. On that days, SunScan measurements have been conducted once, at a single point in time. This has two consequences:

(1) We initially use the daily arithmetic mean of WSN-based LAI estimates for the comparison. Then, additionally to the daily means, a moving average filter is optionally applied, similar to the multi-day aggregation proposed by Qu et al. (2014a) who use a 8 day window and found 3-8 days as a reasonable period to capture the dynamic growth process of leaves. Therefore, we calculate the moving average (referred to as MOVAVG) with a sampling window size of 7, i.e. ± 3 adjacent days, in order to smooth the overall LAI time series and also to bridge gaps where daily means are missing, e.g., due to technical problems.

(2) An option to approximate SunScan LAI estimates on a daily basis in order to enlarge the observation size N for a later correlation analysis is also considered. We tested different approximation methods and finally chose (i) LIN: the simple linear interpolation between individual daily value, and (ii) POLY: a polynomial approximation (degree = 5) as reasonable candidates to approximate the real LAI trajectories. Both methods can optionally also be applied to the daily WSN LAI estimates, complementary to the moving average. The effect of the different approximation methods is exemplarily shown in Figure 10 for both cultivar 1 plots.

In Figure 10(a), the ground truth data for the comparative analysis and its different approximations are visualized. Usually, drought stress leads to a lower LAI maximum (LAI_{max}) that is reached earlier in the growing season as can also be observed in the figure, clearly emphasized by the POLY approximations. For that reason, LAI_{max} is an important parameter of crop physiology. Note that both peaks and the temporary decline of the ROS curve (green) at DOY 146 are caused by occasional irrigation which was conducted in order to prevent excessive drought stress. The corresponding LAI time series obtained by the WSN with data processing and pre-filtering (Fig. 10(b)) already show promising

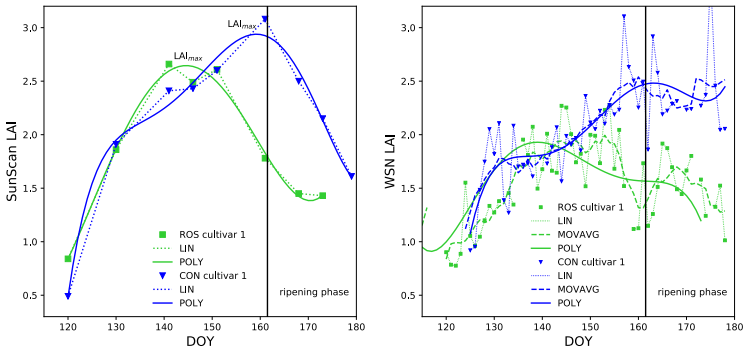

(a) Manually measured SunScan LAI estimates.

(b) Daily averaged WSN LAI estimates.

Figure 10: Approximation of LAI estimates over the wheat growth period for all sensing locations of the deployment (ROS locations are shaded in green, CON in blue).

similarities. However, during the last third of the deployment period (ripening phase), i.e. approximately from DOY 161, there is a systematic discrepancy in the CON LAI curves. The WSN CON time series remains at a high level compared to a clearly decreasing SunScan series. The reason for this discrepancy is that SunScan series actually estimate the GLAI (cf. Sec. 2.4). In contrast, due to fixed sensor locations, the WSN approach is not able to differentiate green from yellow leaves. Neverthelss, the development of GLAI can be entirely monitored by the WSN until LAI_{max} is reached.

5.4. Preliminary LAI Correlation Results

The processing chain presented in the previous subsections creates LAI estimates and enables a preliminary comparative analysis of WSN and SunScan LAI estimates. In the following, results of this analysis are briefly introduced and, at the same time, impacts of different previous processing steps are shown, before being improved by important filter mechanism in the next section.

Due to the GLAI issue, the comparison is limited to the period DOY 120–161 and excludes the ripening phase. Table 2 summarizes the results according to the metrics introduced in Section 4. Here, *naïve* represents the setting with

Table 2: Correlation Evolution – Part I.

	naïve			Preprocessing			Post-processing			w/o sensor 0x8		
Metric	MR	ML	PP	MR	ML	PP	MR	ML	PP	MR	ML	PP
r^2	0.76	0.46	0.71	0.80	0.66	0.82	0.88	0.81	0.82	0.88	0.85	0.78
N	22	158	158	22	149	158	22	160	158	21	155	158
α	1.62	0.83	1.26	1.30	0.93	1.22	1.30	1.19	1.22	1.14	1.10	1.25
β	-0.28	1.04	0.41	-0.04	0.64	0.17	0.03	0.20	0.17	0.25	0.30	0.10
nRMSE	0.62	0.42	0.49	0.34	0.24	0.32	0.31	0.29	0.32	0.08	0.09	0.12

(MR = moving averaged WSN vs. raw SunScan estimates, ML = moving averaged WSN vs. linear approximated SunScan estimates, PP = polynomial approximated WSN vs. SunScan estimates
r^2: coefficient of determination, N: sample size, α: slope , β: intercept)

nearly unprocessed data (only PAR bundles are averaged). Then, this setting is successively extended by minimum PAR threshold (*PARTHRESH*), by applying a priori determined *calibration* factors, by the *median filter* (preprocessing), and finally by the *moving average* on daily scale (post-processing). Moreover, due to the observed deviation of sensor 0x8 (cf. Sec. 5.1), there are two additional settings, one ignoring sensor 0x8 when merging the cultivar 2 samples of the CON plot, and the other one, completely ignoring cultivar 2 CON plot in the comparative analysis. For each setting, three combinations of LAI approximations are considered: *MR*, *ML*, and *PP*, representing the approximations MOVAVG (M), LIN (L) and POLY (P), where the first character belongs to WSN and the second to SunScan LAI time series, respectively.

The core message of the results listed in Table 2 is visualized in Figure 11 that highlights the evolution of correlation quality improvements for different approximation settings. These (preliminary) results show a significant improvement achieved by an adequate processing and, furthermore, already exhibit a high level of correlation.

6. Filtering

An appropriate filtering of raw sensor data is crucial to further improve the quality of our approach and can be integrated in the preprocessing phase of the processing chain as sketched in Figure 5. During the data analysis, we explored and developed various filter mechanisms and present the most important filters

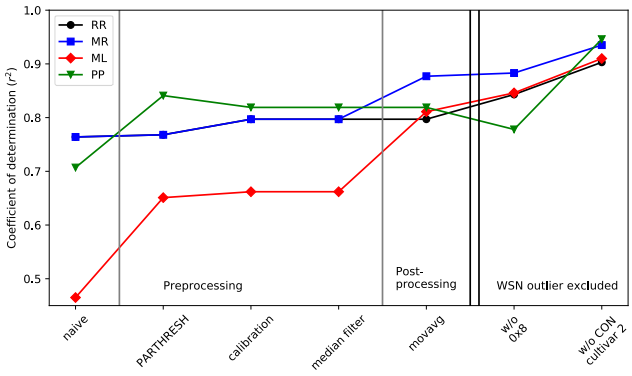

Figure 11: Impact of basic data processing phases on the quality of ground truth correlation.

in this section. First, a generic method is introduced. Then, application-specific approaches are proposed that are tailored to WSN- and radiation-based LAI monitoring.

6.1. ICA Filter

A very powerful technique from the domain of signal processing is the independent component analysis (ICA) that can be applied in order to separate additive subcomponents from a multivariate signal. However, the ICA is a blind source separation, i.e. it works without the aid of additional information about the mixed input signals but also does not provide any information about the separated outputs. Transferred to the PAR time series, our goal is to eliminate undesired interfering signals. Possible reasons of interfering signals are shading effects from the environment or temporal technical failures, for instance, that are assumed to meet the requirements of being non-Gaussion and statistically independent. However, only for the solar irradiance signal captured by the three above reference sensors, the ICA is reasonably applicable and enables a filtering of unintended noise in the reference signal. We use a time window of 7 days for the ICA of the mixed above signals with a zero padding for missing values and identify one output signal as reasonable candidate of an interfering signal. Then, a proper threshold is evaluated and used to create a binary filter. Regarding

the following LAI estimation, the elimination of above reference samples also implicitly discards ground samples since simultaneous pairs are required for LAI determination, cf. Sec. 5.2.

6.2. Assessment-specific Filtering

On the particular site of our deployment, the ROS purposely covers the wheat plots during rainfall periods and affects LAI estimation. Hence, such periods need to be filtered, although we observed only a slight impact of precipitation in the CON plots that often seems to be negligible, e.g., at DOY 145 (Fig. 9(b) in Sec. 5.2). However, the overall precipitation during the deployment was relatively rare and low. Thus, a sound scientific statement on the impact of rain is not possible using our data set. For the RAIN filter, we apply a conservative approximation of hourly weather information leading to a comparative strong binary filter. Note that if accurate information about current precipitation is not available, a raindrop sensor could be easily integrated into the WSN system in order to assist such a rain filter.

The analysis of the probability distribution of multiple PAR readings within a PAR bundle of individual sensor samples shows a very low standard deviation of bundles with occasional outliers. The cause of such outliers is twofold. On the one hand, PAR measurements at low illuminance tend to have lower accuracy, and thus, more variance, particularly in discretized digital readings. Affected sensor samples are mainly already filtered by the *PARTHRES* mechanism in the preprocessing phase. On the other hand, short-term dynamics in the plant stock caused by leaf movements that are primarily triggered by wind results in an increase of the variance. As the latter reason of variance is induced by environmental dynamics, we found a characteristic difference between the variance of bundles gathered within wheat plots and of bundles captured by the above references that are affected by leaf movements.

With regard to the filtering of raw sensor data, a wind filter would be possible if accurate wind information is available for the certain site. However, since wind is the secondary quantity affecting the PAR deviation, we prefer a pure

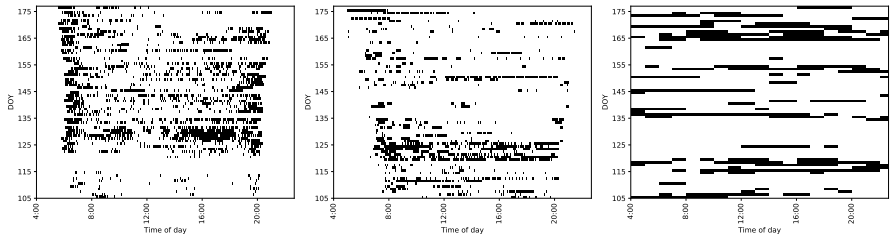

(a) STDPAR filter. (b) ICA filter. (c) RAIN filter.

Figure 12: Filter masks of the proposed filters in a temporal binary matrix representation and their different distributions.

standard-deviation-based filter (referred to as STDPAR filter). Hence, based on the deviation determined for each data stream in the preprocessing phase, we create a sensor-specific binary filter and discard all PAR samples exceeding the threshold. A corresponding filter mask for sensor 0x1 is exemplarily shown in Figure 12(a) along with the filter masks of both previous filters. In each figure, the temporal distribution of filtered intervals (black) can be observed. The STDPAR filter mainly eliminates samples in dawn and dusk periods that tends to be unreliable due to low illuminance as well as samples impacted by wind during the day. The ICA filter mask does not particularly focus on dawn/dusk periods (Fig.,12(b)) and, similar to the RAIN filter (Fig. 12(c)), it has no meaningful pattern.

7. Correlation Results

Starting from the preliminary correlation results of Section 5.4, the impact of each proposed filter and the additional improvement regarding the accuracy and consistency of LAI time series are again evaluated by a comparative analysis to SunScan LAI estimates. The results are quantified in Table 3 and Figure 13. It turns out that the proposed filtering is an appropriate fine-tuning optimization that has a comparatively lower impact than the basic data processing. It results in a slight, yet effective increase of the already high determination co-

Table 3: Correlation Evolution – Part II.

	processed			+ ICA filter			+ RAIN filter			+ STDPAR filter		
Metric	MR	ML	PP	MR	ML	PP	MR	ML	PP	MR	ML	PP
r^2	0.88	0.81	0.82	0.89	0.82	0.82	0.89	0.83	0.83	0.91	0.85	0.84
N	22	160	158	22	160	158	22	156	158	22	140	158
α	1.30	1.19	1.22	1.25	1.16	1.16	1.27	1.17	1.19	1.33	1.22	1.23
β	0.03	0.20	0.17	0.14	0.26	0.28	0.11	0.26	0.25	0.05	0.20	0.22
nRMSE	0.31	0.29	0.32	0.08	0.10	0.10	0.08	0.10	0.10	0.07	0.09	0.10

(MR = moving averaged WSN vs. raw SunScan estimates, ML = moving averaged WSN vs. linear approximated SunScan estimates, PP = polynomial approximated WSN vs. SunScan estimates
r^2: coefficient of determination, N:sample size, α: slope , β: intercept)

efficient (Fig. 13(a)). At the same time, the overall data set is further reduced by even more samples using the filter operations than by the prior preprocessing (cf. Fig. 13(b)).

In addition, Figure 14 highlights two correlation properties of the proposed filtering. First, concerning the accuracy of our approach represented by the nRMSE, a clear trend can be observed (Fig. 14(a)). The higher the improvement of the correlation achieved by successive filtering, the higher is also the accuracy. Second, the linear regressions of all individual correlation pairs with different approximations result in a very low interception (Fig. 14(b)). Thus, in order to neglect this additive correlation parameter and to focus on the slope, the linear regressions are forced to the origin (α_0). The results are also integrated into the figure (unfilled markers) and are accumulated around a slope of 1.324 as emphasized by the α_0 boxplot.

8. Discussion & Comparison to Related Work

8.1. LAI Calibration

For a consistent LAI estimation using our radiation-based approach and the formula in Equation 1 (Sec. 2.3), a reliable calibration factor ω is required. This factor is plant- and site-specific and is related to the so-called extinction coefficient. With regard to our approach, this calibration factor has already been successfully determined for maize (cf. Bauer et al., 2016). So far, a preliminarily

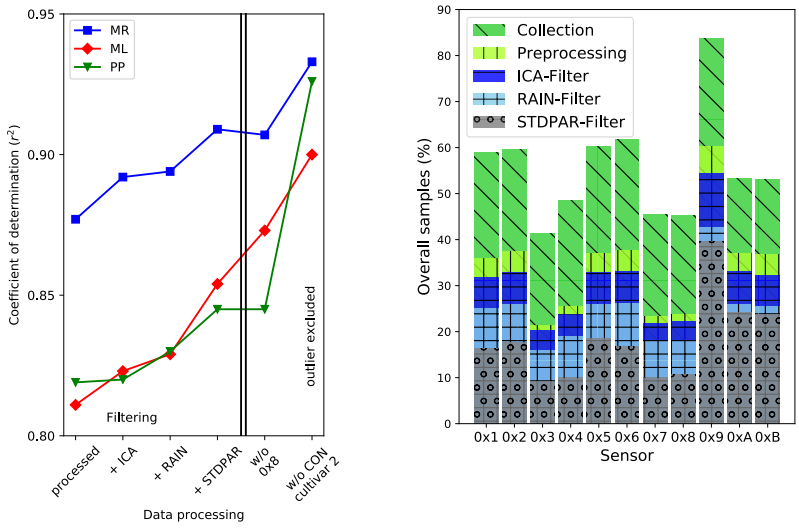

(a) Evolution of correlation.

(b) Data reduction due to filtering. The references for the respective percentage values are the theoretical maximum number of samples, cf. *success rate* in Fig. 4.

Figure 13: Impact of filtering on the quality of ground truth correlation.

assignment of $\omega_{initial} = 1.24$ was used. Taking the fully-processed and filtered LAI estimates and different approximation setups into account, a reasonable assignment for wheat cultivars can now be determined. We found that in all approximation setups and across all filter steps in Table 3, α is relatively constant. The statistics of the corresponding boxplot in Fig 14(b) gives the factor $\alpha_0 = 1.324$. This value results in $\omega_{wheat} = \alpha_0\, \omega_{initial} \approx 1.324 \cdot 1.24 \approx 1.64$.

Using this calibration factor, LAI estimates can be finally adjusted and meaningful LAI trajectories can be derived. Figure 15 compares WSN-derived LAI time series (moving average) with series from manually gathered SunScan estimates as ground truth. Here, each subfigure corresponds to the according approximation pair considered in Section 7. Independent of the particular approximation setup, the comparison reveals that our approach can greatly fit the dynamic wheat growth process. Moreover, change tendencies induced by intentional drought stress in the ROS plots and even cultivar-specific differences are

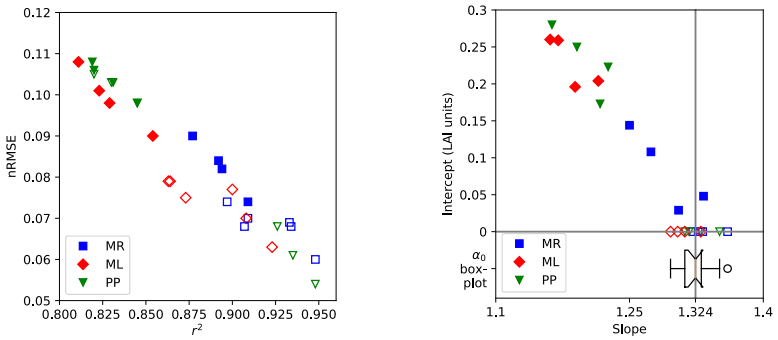

(a) Increasing the correlation also implies nRMSE reduction. Solid markers represent results from all wheat plots, unfilled markers according information but excluding WSN outliers (sensor 0x8 or CON cultivar 2).

(b) Slope and intercept of different approximation setups extended by a boxplot summarizing all slopes that were forced through the origin (indicated by unfilled markers).

Figure 14: Correlation properties of processed and filtered LAI series.

captured by the WSN.

In accordance to the findings of Qu et al. (2014a), the multi-day aggregation using the MOVAVG approach enables the most reasonable results. Regarding this approach, we found that the very high correlation with raw SunScan estimates ($r^2 = 0.91$, Fig. 15(a)) still remains on a level that is usable in practice ($r^2 = 0.85$, Fig. 15(b)) when the sample size N for the correlation is artificially increased by the linear interpolation of SunScan estimates. However, we should note that, despite of the wide scientific use and acceptance, the accuracy of commercial LAI instruments and plant canopy analyzers under certain conditions are discussed controversially in literature (e.g., Wilhelm et al., 2000; Bréda, 2003; Jonckheere et al., 2004; Garrigues et al., 2008). Thus, using ground truth LAI values assessed by the SunScan device introduces a certain error to our comparative analysis. Hence, an absolute scientific evaluation on the accuracy of our approach is hardly possible.

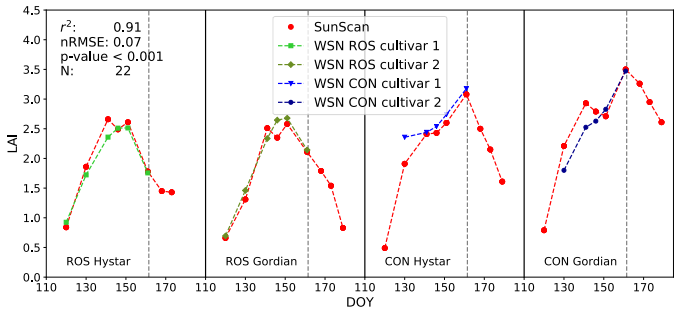

(a) WSN-MOVAVG vs. SunScan-RAW.

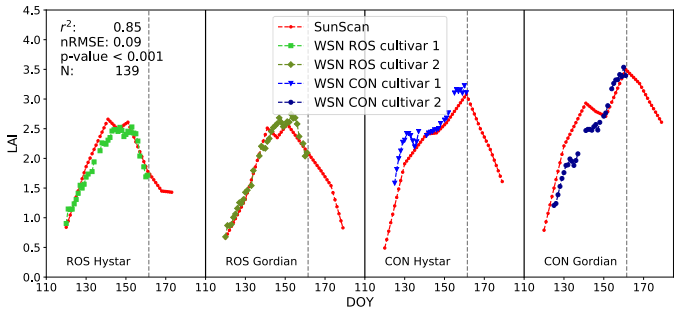

(b) WSN-MOVAVG vs. SunScan-LIN.

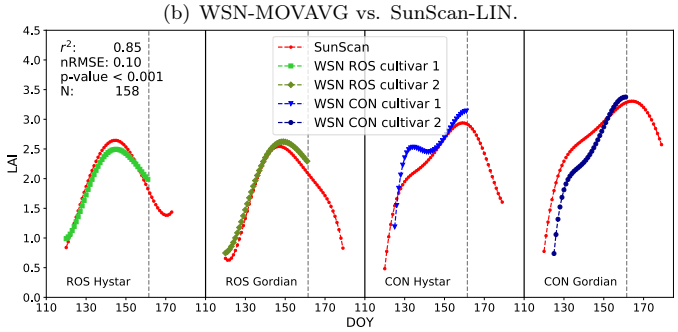

(c) WSN-POLY vs. SunScan-POLY.

Figure 15: Final post-processed and filtered WSN LAI trajectories in comparison with SunScan ground truth using different approximation setups.

8.2. Limitations of Our Approach

The simplified model of Monsi-Seaki (Monsi and Saeki, 1953) used to derive LAI information in our approach, abstracts from certain factors that influence this derivation and, thus, has its limitations. In our approach, this abstraction

is addressed using the correction factor ω and the daily averaging of LAI estimates that both result in promising LAI trajectories and a high agreement to the SunScan reference. Nevertheless, we observed a daily pattern of LAI time series on sunny days (cf. Fig. 9(a) in Sec. 5.2). This pattern is well-known and primarily caused by the SZA θ_s since the incident angle of sunrays has a direct impact on the path length $S(\theta_s)$ that sunrays travel through the canopy to the ground. Assuming that the canopy is horizontally large enough, $S(\theta_s)$ can be expressed as $S(\theta_s) = cos(\theta_s)^{-1}$. Taking this into account, the simplified LAI calculation of Equation 1 can be extended by this trigonometric function resulting in a product that is referred to as contact number κ (Lang and Yueqin, 1986). Moreover, the SZA is not the only factor that influences LAI estimation. Hence, Equation 1 can be further extended by the species-specific G-function $G(\theta_L, \theta_s)$ that also takes the MLA θ_L into account (cf. Weiss et al., 2004). This is generally expressed as:

$$LAI = \frac{\kappa(\theta_s)}{G(\theta_L, \theta_s)} = -cos(\theta_s)\ ln\left(\frac{\overline{B}}{\overline{A}}\right)\ G(\theta_L, \theta_s)^{-1}. \tag{2}$$

Unfortunately, the G-function is usually unknown which makes it difficult to estimate an absolute LAI. However, under the assumption of spherical distribution of canopy leave angles, it has been analytically shown that for a particular zenith angle $\theta_s = 57.5°$, this function is independent of θ_L and constant with approx. 0.5 (Wilsoni, 1963), resulting in:

$$LAI = -2\ cos(57.5)\ ln\left(\frac{\overline{B}}{\overline{A}}\right). \tag{3}$$

8.3. Comparison

As already mentioned in Section 2.2, there is only a limited amount of directly related work regarding WSN-based LAI assessment. Li et al. (2015) propose a novel sensor type that uses DHP for indirect LAI assessment. However, their sensor device is much more complex and less cost-effective, thus, not suitable for large-scale deployments. Only a few comparable real-world deployments in agricultural context exist, most notably LAINet (Qu et al., 2014b,a)

and the monitoring system proposed by Shimojo et al. (2013). Generally, our experiences with real-word deployment is consistent to practical challenges reported in the literature. The numerical quality (represented by r^2 and nRMSE) of our results can clearly compete with related WSN approaches and also with more complex techniques that use more powerful devices such as DHP (Ryu et al., 2012), for instance. Both approaches mentioned above also produce LAI trajectories but with lower temporal resolution and differ from our approach in terms of the sensing device and/or in terms of application. Furthermore, both approaches do not take a bundle of multiple consecutive PAR readings as appropriate filter into account. Shimojo et al. (2013) use a similar device and a single-angle algorithm for greenhouse monitoring but without an optical bandpass filter. In contrast, Qu et al. (2014a) developed a more complex device consisting of multiple sensors. Following a multi-sensor and -angle algorithm, their approach is used for forest LAI estimation and also to collect ground LAI of maize for the validation of remote sensing products (Qu et al., 2014b).

For a comparison to related approaches, we also implemented the single-angle LAI estimation according to Equation 3, referred to as *LAI-575* and also the sensing strategy introduced by Shimojo et al. (2013). In order to cope with the weather impact, the authors propose an algorithm for a proper measurement timing decision based on empirical knowledge. On sunny days, PAR measurements should be taken just before direct sunlight reaches the overfoliage (e.g., 07:00) whereas on overcasted days periods should be used for the measurements when the light intensity remains on a constant level (e.g., 09:00). We implemented Shimojo's approach and, using the DWD weather information, we adapted the proposed timing to our time zone and region.

However, the fixed measurement timing was found to be inappropriate for our long-term deployment. We consequently adapted the timing to seasonal variations of the sun path. By this means, a significant performance increase could be achieved that is however still outperformed by our approach (denoted as *LAI-wheat*) as visualized by Figure 16. A possible reason for this mismatch are the different sensor devices and that, due the application area in green-

house monitoring, Shimojo's approach neglects wind effects that are addressed by our approach. Furthermore, the amount of cloudy days is much lower in our deployment because of different season and region which might make this approach not feasible for a fine-grained wheat LAI assessment. Moreover, Figure 16 shows that our approach also outperforms the single-angle approach *LAI-575* that qualitatively comes closer to our approach. The single-angle algorithm has the advantage of maximal energy efficiency because it requires to measure the transmittance solely in one particular SZA. But at the same time, it is generally more impacted by weather factors.

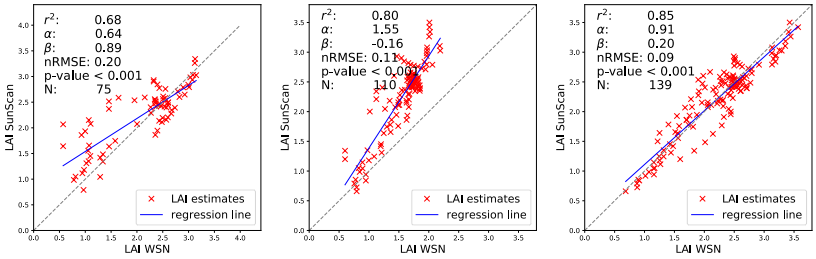

(a) *LAI-Shimojo.* (b) *LAI-575.* (c) *LAI-wheat.*

Figure 16: Comparison with related LAI assessment approaches in WSNs, exemplarily shown for the particular approximation setup WSN-MOVAVG vs. SunScan-LIN.

8.4. WSN-related Issues

The LAI-specific *STDPAR* filter proposed in Section 6.2, could be applied in a future WSN for an early detection of noisy and unusable PAR bundles directly on the sensing devices. Hence, it could assist the in-situ rating of a specific sample and the decision of forwarding or discarding. That would significantly reduce communication cost and, thus, contribute to energy-efficiency which is one of the fundamental challenges for WSNs.

In the presented deployment, the sampling strategy is an intended oversampling and the question of an adequate LAI sampling interval that achieves a reasonable energy-accuracy tradeoff is still an open issue and will be part of our future work. Nevertheless, the total data size collected using the oversampling

strategy is less than 5 MB/sensor during the entire deployment. Thus, the produced data is absolutely manageable. Regarding forwarding to the backbone network (e.g., Internet), the resulting daily reports (750 kB/day) could be further reduced by the proposed in-situ filtering as well as by existing aggregation and compression algorithms.

9. Conclusion

In this paper, we used our radiation-based LAI sensor prototypes in a long-term WSN deployment for a continuous monitoring of crop LAI. We demonstrated the general feasibility and the great potential of our system. A cultivar- and site-specific correction factor was successfully determined for winter wheat and we showed that our approach enables temporal fine-grained LAI trajectories. These trajectories are found to yield a high accuracy and, thus, to fit the dynamic growth process of crops. Moreover, cultivar-specific differences and change tendencies in this process can be reliably detected with our system as shown by experimental results in the rain-out shelter environment with intentionally induced drought stress.

For a purposeful processing of WSN data, we applied standard filtering mechanism and multi-day averaging, but also introduced a novel filter for outdoor environments that is able to eliminate noise induced by small-scale dynamics in the plant stock. Furthermore, a comparison to related approaches showed that for high-quality LAI profiles, it is worth considering multiple incident angles across each day in the process of LAI assessment. However, a reasonable quantity and specification of important angles for our approach is still missing. Therefore, a comprehensive evaluation of adequate sensing strategies is planned in our future work. We will use the data from this deployment to further investigate different sensing strategies and the trade-off between the sampling rate and energy consumption in order to significantly reduce the required sampling rate. By doing so, our goal is to answer two important questions: How often do sensors have to sample the PAR and when is the most efficient time to do that?

References

Akyildiz, I. F., Su, W., Sankarasubramaniam, Y., Cayirci, E., Mar. 2002. Wireless Sensor Networks: A Survey. Computer Networks 38 (4), 393–422.

Bauer, J., Aschenbruck, N., 2018. Design and Implementation of an Agricultural Monitoring System for Smart Farming. In: Proc. of the IEEE IoT Vertical and Topical Summit for Agriculture. Monteriggioni, Italy, pp. 1–6.

Bauer, J., Siegmann, B., Jarmer, T., Aschenbruck, N., 2016. On the Potential of Wireless Sensor Networks for the In-Situ Assessment of Crop Leaf Area Index. Computers and Electronics in Agriculture 128, 149–159.

Boegh, E., Soegaard, H., Broge, N., Hasager, C. B., Jensen, N. O., Schelde, K., Thomsen, A., 2002. Airborne multispectral data for quantifying leaf area index, nitrogen concentration, and photosynthetic efficiency in agriculture. Remote Sensing of Environment 81 (2–3), 179–193.

Bréda, N., 2003. Ground-based measurements of leaf area index: a review of methods, instruments and current controversies. Journal of Experimental Botany 54, 2403–2417.

Carter, G. A., 1994. Ratios of leaf reflectances in narrow wavebands as indicators of plant stress. International Journal of Remote Sensing 15 (3), 697–703.

Garrigues, S., Shabanov, N., Swanson, K., Morisette, J., Baret, F., Myneni, R., 2008. Intercomparison and sensitivity analysis of Leaf Area Index retrievals from LAI-2000, AccuPAR, and digital hemispherical photography over croplands. Agricultural and Forest Meteorology 148 (8–9), 1193–1209.

Jonckheere, I., Fleck, S., Nackaerts, K., Muys, B., Coppin, P., Weiss, M., Baret, F., 2004. Review of methods for in situ leaf area index determination: Part I. Theories, sensors and hemispherical photography. Agricultural and Forest Meteorology 121 (1–2), 19–35.

Lang, A., Yueqin, X., 1986. Estimation of leaf area index from transmission of direct sunlight in discontinuous canopies. Agricultural and Forest Meteorology 37 (3), 229–243.

Li, X., Liu, Q., Yang, R., Zhang, H., Zhang, J., Cai, E., 2015. The Design and Implementation of the Leaf Area Index Sensor. Sensors 15 (3), 6250–6269.

Mo, L., He, Y., Liu, Y., Zhao, J., Tang, S.-J., Li, X.-Y., Dai, G., 2009. Canopy closure estimates with GreenOrbs: sustainable sensing in the forest. In: Proc. of the 7th ACM Conference on Embedded Networked Sensor Systems (SenSys). Berkeley, CA, USA, pp. 99–112.

Monsi, M., Saeki, T., 1953. Über den Lichtfaktor in den Pflanzengesellschaften und seine Bedeutung für die Stoffproduktion. Japanese Journal of Botany 14, 22–52.

Qu, Y., Han, W., Fu, L., Li, C., Song, J., Zhou, H., Bo, Y., Wang, J., 2014a. LAINet – A wireless sensor network for coniferous forest leaf area index measurement: Design, algorithm and validation. Computers and Electronics in Agriculture 108, 200–2089.

Qu, Y., Zhu, Y., Han, W., Wang, J., Ma, M., Feb 2014b. Crop Leaf Area Index Observations With a Wireless Sensor Network and Its Potential for Validating Remote Sensing Products. IEEE Journal of Selected Topics in Applied Earth Observations and Remote Sensing 7 (2), 431–444.

Rehman, A.-u., Abbasi, A. Z., Islam, N., Shaikh, Z. A., 2014. A Review of Wireless Sensors and Networks' Applications in Agriculture. Computer Standards & Interfaces 36 (2), 263–270.

Ryu, Y., Verfaillie, J., Macfarlane, C., Kobayashi, H., Sonnentag, O., Vargas, R., Ma, S., Baldocchi, D. D., 2012. Continuous observation of tree leaf area index at ecosystem scale using upward-pointing digital cameras. Remote Sensing of Environment 126 (0), 116 – 125.

Schittenhelm, S., Kraft, M., Wittich, K.-P., 2014. Performance of winter cereals grown on field-stored soil moisture only. European Journal of Agronomy 52, 247–258.

Shimojo, T., Tashiro, Y., Morito, T., Suzuki, M., Lee, D., Kondo, I., Fukuda, N., Morikawa, H., 2013. A Leaf Area Index visualization method using wireless sensor networks. In: Proc. of Int. Conf. on Instrumentation, Control, Information Technology and System Integration Conference (SICE). Nagoya, Japan, pp. 2082–2087.

Vasisht, D., Kapetanovic, Z., Won, J.-h., Jin, X., Chandra, R., Kapoor, A., Sinha, S. N., Sudarshan, M., Stratman, S., 2017. Farmbeats: An IoT Platform for Data-driven Agriculture. In: Proc. of the 14th USENIX Conference on Networked Systems Design and Implementation (NSDI'17). Boston, MA, USA, pp. 515–528.

Weiss, M., Baret, F., Smith, G., Jonckheere, I., Coppin, P., 2004. Review of methods for in situ leaf area index (LAI) determination: Part II. Estimation of LAI, errors and sampling. Agricultural and Forest Meteorology 121 (1–2), 37 – 53.

Wilhelm, W., Ruwe, K., Schlemmer, M. R., 2000. Comparison of three leaf area index meters in a corn canopy. Crop Science 40 (4), 1179–1183.

Wilsoni, J., 1963. Estimation of foliage denseness and foliage angle by inclined point quadrats. Australian Journal of Botany 11 (1), 95–105.

Yuan, Y., Li, S., Wu, K., Jia, W., Peng, Y., 2009. FOCUS: A cost-effective approach for large-scale crop monitoring with sensor networks. In: Proc. of the Int. Conf. on Mobile Adhoc and Sensor Systems (MASS). Macao, China, pp. 544–553.